Electronic Structure and Nature of the Ground State of the Mixed-Valence Binuclear Tetra(μ-1,8-naphthyridine-*N*,*N*′)-bis(halogenonickel) Tetraphenylborate Complexes: Experimental and DFT Characterization

Alessandro Bencini,* Elisabetta Berti, Andrea Caneschi, Dante Gatteschi, Elisa Giannasi, and Ivana Invernizzi[a]

Abstract: The ground state electronic structure of the mixed-valence systems $[Ni_2(napy)_4X_2](BPh_4)$ (napy = 1,8-naphthyridine; X = Cl, Br, I) was studied with combined experimental (X-ray diffraction, temperature dependence of the magnetic susceptibility, and high-field EPR spectroscopy) and theoretical (DFT) methods. The zero-field splitting (zfs) ground $S = 3/2$ spin state is axial with $|D| \approx 3\ cm^{-1}$. The iodide derivative was found to be isostructural with the previously reported bromide complex, but not isomorphous. The compound crystallizes in the monoclinic system, space group $P2_1/n$, with $a = 17.240(5)$, $b = 26.200(5)$, $c = 11.340(5)$ Å, $\beta = 101.320(5)^\circ$. DFT calculations were performed on the $S = 3/2$ state to characterize the ground state potential energy surface as a function of the nuclear displacements. The molecules can thus be classified as Class III mixed-valence compounds with a computed delocalization parameter, $B = 3716$, 3583, and 3261 cm^{-1} for the Cl, Br, and I derivatives, respectively.

Keywords: density functional calculations · double exchange interaction · mixed-valent compounds · X-ray diffraction

Introduction

Mixed-valence transition metal complexes, that is, systems in which metal ions have at least two different oxidation states, have been, and are currently, investigated because they exhibit a number of peculiar properties of relevance in different fields of science including chemistry, biology, and physics.[1–3] Mixed-valence species can be regarded as being formed by two or more transition metal centers bearing fractional formal charges, or, better, by integer valence-localized centers and "extra" electron(s) that can hop from one center to the other.[4] External perturbations, like electric fields, can lead to a localization of the unpaired electron, and nuclear reorganization may also stabilize a localized system, that is, can trap the electron on one site. Electron delocalization can be effective only in symmetric geometries, and the interplay between electronic and nuclear motions (*vibronic coupling*) is an important characteristic of the mixed-valence systems.[5]

Among the appealing properties of mixed-valence compounds, magnetism is a particularly relevant one. In particular it is now well established that when the two oxidation states are magnetic, if the electron can hop quickly from one center to the other it stabilizes a ferromagnetic ground state, due to the so-called *spin-dependent delocalization* or *double exchange*.[6] Double-exchange effects have now been observed in such diverse materials as the manganite perovskites, which show the phenomenon of colossal magneto resistance[7] and the iron–sulfur proteins.[8]

In the last few years much progress has been made, from the theoretical point of view, in the understanding of the nature of the double exchange in mixed-valence compounds, and certainly the simple binuclear cation $[Ni_2(napy)_4X_2]^+$ (napy = 1,8-naphthyridine; X = Cl, Br, I)[9] has provided much insight into the double-exchange phenomenon. The bromide derivative showed a structure[9a] reminiscent of that of copper(II) acetate,[10] with four napy molecules bridging two nickel ions, and two halides in the axial position (Scheme 1). The two nickel ions bear a formal charge of 3+, therefore they can be formally considered as one nickel(II) and one nickel(I). In the X-ray crystal structure the two metal ions showed practically identical bond lengths and angles, suggesting that also this compound corresponds to Class III of the classification of Robin and Day[11] of mixed-valence compounds. The magnetic properties of $[Ni_2(napy)_4Br_2]^+$ revealed that the ground spin state of the system is a quartet state, with no evidence of thermally populated doublets.[9] Since nickel(II), $3d^8$, has $S = 1$ and nickel(I), $3d^9$, has $S = 1/2$, it was suggested that the origin of the strong ferromagnetic ex-

[a] Prof. A. Bencini, Dipl.-Chem. E. Berti, Dr. A. Caneschi, Prof. D. Gatteschi, Dipl.-Chem. E. Giannasi, Dr. I. Invernizzi
Dipartimento di Chimica, Polo Scientifico dell'Università di Firenze
via della Lastruccia 3, 50019 Sesto Fiorentino (FI) (Italy)
Fax: (+39) 055-4573372
E-mail: alessandro.bencini@unifi.it

0947-6539/02/0816-3660 $ 20.00+.50/0 *Chem. Eur. J.* **2002**, *8*, No. 16

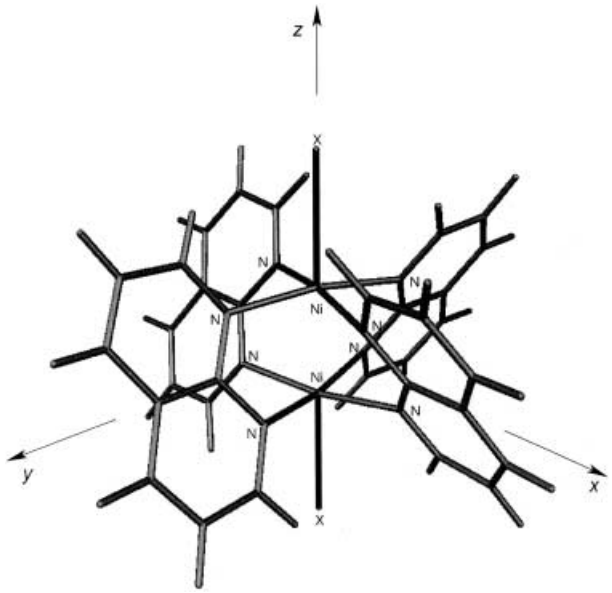

Scheme 1.

change is the double exchange allowed by the fast electron hopping of one unpaired electron between the two sites.[9c, 11]

Although the physical properties of $[Ni_2(napy)_4Br_2]^+$ have been extensively studied,[6c, 9, 11] several points remain obscure in the exact mechanism responsible for the double exchange, for example the assignment of the visible spectrum and, in the magnetic properties, in particular the zero-field splitting (zfs) of the quartet spin state. In recent years it has become possible to analyze in much more detail the magnetic properties of mixed-valence compounds both experimentally and theoretically. For the former it has become possible to routinely use extremely low temperatures and high field EPR and HF-EPR spectroscopies,[13] to fully characterize the magnetic properties of the ground state. For the latter, DFT now allows one to calculate exchange and double-exchange contributions.[14] In particular, DFT was found of invaluable help to characterize the nature of the potential energy surface (PES) of the ground and next excited states and to allow the classification of several mixed valence systems.[15]

We therefore decided to undertake a full program of deep characterization of the $[Ni_2(napy)_4X_2]^+$ ions to shed light on the mechanism responsible for double exchange in simple magnetic compounds. For this purpose, we determined the X-ray crystal structure of the iodide derivative, in order to have additional experimental evidence of the Class III nature of the $[Ni_2(napy)_4X_2]^+$ ions; we measured the magnetic susceptibility of the compounds with X = Cl, Br, I down to 2 K to obtain information on the zero-field splitting of the ground quartet state, and with the same goal we recorded their HF-EPR spectra. Finally we performed DFT calculations to gain quantitative information on the double-exchange mechanism.

Results and Discussion

A common qualitative explanation, based on the localized description of the electronic structure of mixed-valence complexes, introduces the concept of the transfer integral t_{ab}, also called H_{ab}, or β, in electron transfer models, which determines the kinetic constant of the electron transfer.[4, 5] The energy level scheme for d^8 and d^9 ions in square pyramidal coordination environments are shown in Scheme 2 in the active electron approximation, that is, neglecting all the doubly occupied orbitals. The magnetic orbitals are indicated as d_{z^2} and $d_{x^2-y^2}$, and have σ and δ symmetry, respectively, in a diatomic Ni_2 molecule. If one electron of the originally d^9 ion hops from the d_{z^2} orbital to the analogous one of the d^8 site it must keep its spin antiparallel to that of the other electron in the d_{z^2} orbital, thus stabilizing a quartet spin state like an effective ferromagnetic coupling between localized d^8 and d^9 ions. An easier picture is drawn in term of holes (Scheme 2, upper right) in which only the hole localized in the σ orbital can hop between the two centers. The transfer integral can therefore be written $t_{ab} = 2 < \sigma_A | H | \sigma_B >$.[12] More information about the electron transfer mechanism can be obtained using a molecular orbital picture of the electronic structure of the mixed-valence systems, which in the simplest model of three active electrons is shown in the bottom of Scheme 2. The bonding interaction is large for the σ-type orbitals that give rise to the σ_g and σ_u MOs. In the hole formalism two quartet states are obtained [Eq. (1)], the energy difference of which is exactly $2\,t_{ab}$.

$$\psi_u = |\,\delta_g^1\delta_u^1\sigma_g^1\,|\;;\psi_g = |\,\delta_g^1\delta_u^1\sigma_u^1\,| \qquad (1)$$

Hence, considering only one electron term in the interaction Hamiltonian, this is the energy difference between the σ_g and σ_u MOs. This energy difference can be generally measured, in Class III systems, from an intense transition in the visible region, which is responsible for the intense color of these compounds. An equivalent description can be obtained, at the same level of approximation, applying the common Wolfsberg-Helmholtz approximation[16] since the transfer integral can be written as Equation (2) where S_{ab} is the overlap integral between the localized $|\sigma_A>$ and $|\sigma_B>$ orbitals with energies ε_a and ε_b respectively.

$$t_{ab} = kS_{ab}\frac{\varepsilon_a + \varepsilon_b}{2} \qquad (2)$$

Using the MO approach one can relate the magnitude of the transfer integral to the chemical concept of bonding interactions. It is also apparent that electron transfer between magnetic ions includes two types of bonding interactions: a rather weak one between the δ magnetic orbitals and a stronger one between the σ orbitals. The first interaction can tune the magnetic exchange while the second one can give rise to electron delocalization. It is a well-known result for binuclear species that the highest spin state of the molecule can be the ground state even in the presence of antiferromagnetic interactions between the magnetic centers when these interactions are overcome by a strong transfer integral, that is, by strong bonding between a couple of magnetic orbitals. The above treatment neglects electron correlation, except that included in the antisymmetrization of the wave function, and can be considered only as a first-order approach to the electron transfer phenomenon.[17] Any theoretical

  0947-6539/02/0816-3661 $ 20.00+.50/0

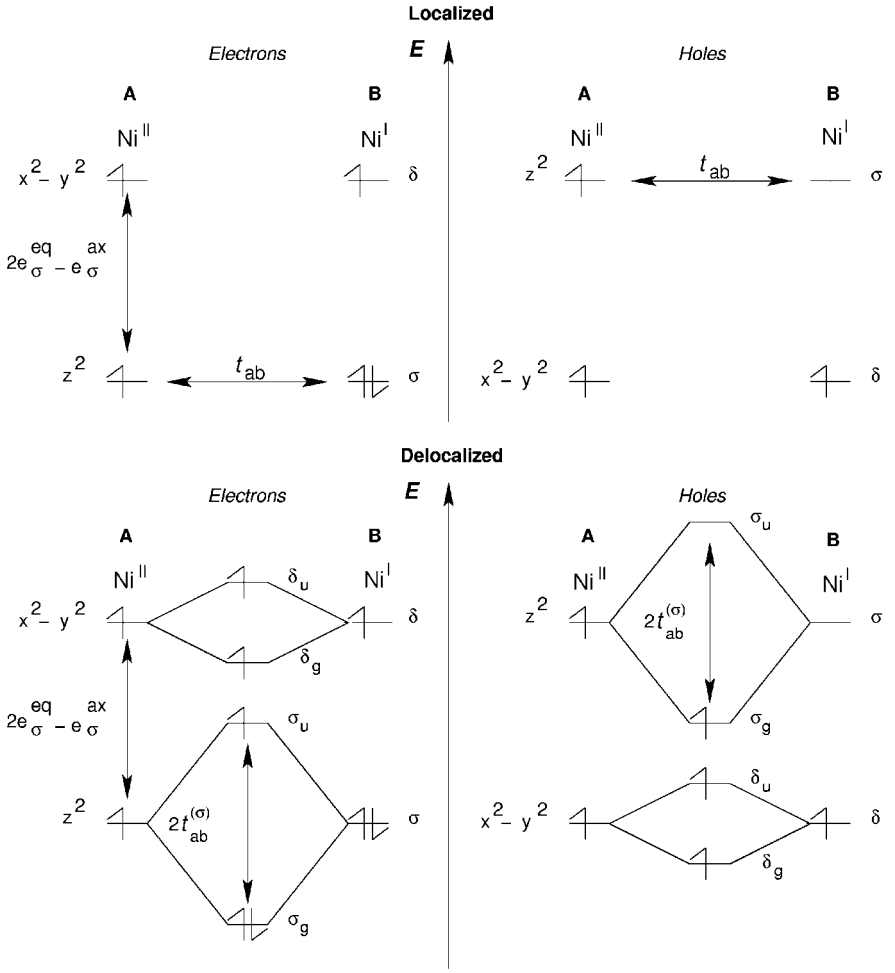

Scheme 2. The energy level scheme for d^8 and d^9 ions in square-pyramidal coordination environments.

model that has to be applied to characterize mixed-valence compounds must therefore handle electron correlation at a reasonable level of accuracy and be able to calculate large molecular aggregates.

Experimentally, it is customary to write the energies of the spin states arising from the double-exchange interaction[18] as in Equation (3), where + and − indicates the two spin states arising from the interaction (for example, the states in Eq. 1), J is the magnetic exchange coupling constant, and B is the double-exchange parameter [Eq. (4)], where S_0 is the spin of the magnetic center in the absence of the "extra" electron.[19]

$$E_{\pm}=\frac{J}{2}S(S+1)\pm B\left(S+\frac{1}{2}\right) \quad (3)$$

$$B=\frac{t_{ab}}{2S_0+1} \quad (4)$$

In the present case, $S=3/2$, 1/2. It must be stressed at this point that the measurement of the temperature dependence of the magnetic susceptibility alone does not permit, in the general case, the independent estimation of J and B, since when $B>J$, one can measure the energy difference between the ground state and a few of the low-lying excited states, sharing the same symmetry (+ or −): therefore J and B are strongly correlated. The independent measurement of B from the electronic spectra requires an assignment, which can be performed only using adequate MO theories.

X-ray crystal structure of $[Ni_2(napy)_4I_2]B(C_6H_5)_4$: The compound is not isomorphous with the bromide derivative, the structure of which was previously reported ($a=9.931(3)$, $b=32.311(8)$, $c=16.535(9)$ Å, $\beta=101.5(3)^\circ$),[9a] but the molecular structures of the two compounds are very similar to each other. The structure of the binuclear $[Ni_2(napy)_4I_2]^+$ ion is shown in Figure 1 and some relevant bond lengths and angles are given in Table 1, where they are compared to the corresponding data of the bromide derivative. The coordination environments of the nickel ions are close to each other, with a rather short nickel–nickel distance, 2.405(1) and 2.421(5) Å for I and Br, respectively. Contrary to the bromide derivative, the two nickel–iodide distances show some asymmetry (2.884(1) versus 2.972(1) Å), but the average nickel–nitrogen distances are identical within error for Ni1 and Ni2 (2.097(5) and 2.090(5) Å respectively). These values compare well with those observed in the bromide derivative (2.09(2) and 2.12(3) Å), although the nickel-nickel distance is shorter than in nickel metal (2.49 Å), indicating some direct metal–metal interaction. The coordination of each Ni ion is a

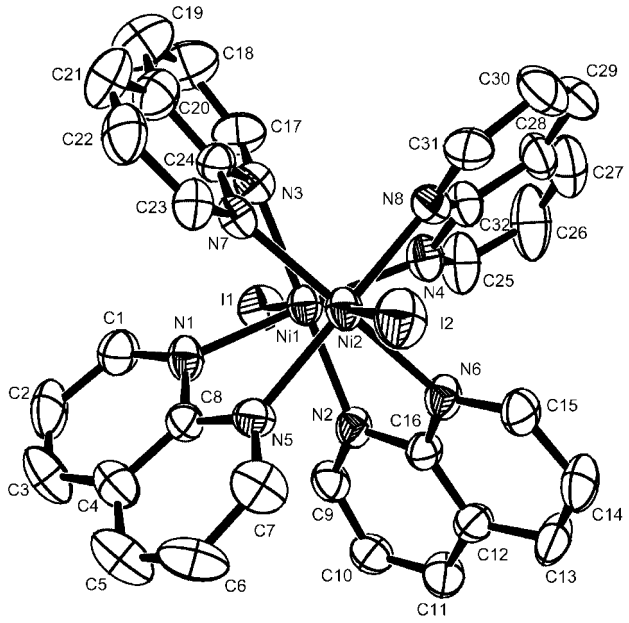

Figure 1. Structure of the $[Ni_2(napy)_4I_2]^+$ ion (ORTEP view).

0947-6539/02/0816-3662 $ 20.00+.50/0 *Chem. Eur. J.* **2002**, *8*, No. 16

Table 1. Selected bond lengths [Å] and angles [°] for $[Ni_2(napy)_4X_2](BPh_4)$.

I1–Ni1	2.885(1)				
I2–Ni2	2.972(1)	Ni1–Ni2	2.405(1)	Ni1–N1	2.115(5)
Ni1–N2	2.083(5)	Ni1–N3	2.107(5)	Ni1–N4	2.082(5)
Ni2–N5	2.098(5)	Ni2–N6	2.084(5)	Ni2–N7	2.095(5)
Ni2–N8	2.086(5)	N4-Ni1-N2	89.4(2)	N4-Ni1-N3	92.1(2)
N2-Ni1-N3	171.4(2)	N4-Ni1-N1	171.0(2)	N2-Ni1-N1	88.4(2)
N3-Ni1-N1	88.7(2)	N4-Ni1-Ni2	85.3(1)	N2-Ni1-Ni2	85.4(1)
N3-Ni1-Ni2	86.3(1)	N1-Ni1-Ni2	85.8(1)	N4-Ni1-I1	96.1(1)
N2-Ni1-I1	93.0(1)	N3-Ni1-I1	95.3(1)	N1-Ni1-I1	92.7(1)
Ni2-Ni1-I1	177.8(4)	N6-Ni2-N8	88.6(2)		
N6-Ni2-N7	171.6(2)	N8-Ni2-N7	90.6(2)	N6-Ni2-N5	89.1(2)
N8-Ni2-N5	171.6(2)	N7-Ni2-N5	90.6(2)	N6-Ni2-Ni1	85.7(1)
N8-Ni2-Ni1	86.6(2)	N7-Ni2-Ni1	85.8(1)	N5-Ni2-Ni1	85.2(1)
N6-Ni2-I2	93.6(1)	N8-Ni2-I2	94.4(1)	N7-Ni2-I2	94.9(1)
N5-Ni2-I2	93.8(1)				

distorted square pyramid with the average I-Ni-N angle of 94° equal to that observed in the bromide derivative. The overall geometry of the coordination polyhedron is a bicapped tetragonal antiprism, the average twist angle, τ, between the two tetragonal pyramids is 28°, close to the value of 25° observed in the bromide derivative.

Magnetic measurements: The temperature dependence of the magnetic susceptibility of polycrystalline powder samples of the iodide and chloride derivatives was measured in the temperature range 150–2.4 K (Figure 2). For both compounds χT remains essentially constant at approximately 2.19 emu mol^{-1} K in the temperature range 150–20 K. The value of the effective magnetic moment, $\mu_{eff} = 4.18\,\mu_B$, agrees with a ground $S = 3/2$ state with $g \approx 2.16$. Below 20 K a rapid decrease of χT was measured, which was attributed to the zero-field splitting (zfs) of the quartet spin state. Assuming an axial zfs Hamiltonian, $D\left[S_z^2 - \frac{S(S+1)}{3}\right]$, the ground quartet state is split into two Kramers doublets separated in energy by $2D$, and the magnetic susceptibilities are expected to be anisotropic and should follow Equation (5), where the symbols have their usual meaning.[20]

$$\chi_{\parallel} = \frac{Ng_{\parallel}^2\mu_B^2(1+9e^{-2D/kT})}{4kT(1+e^{-2D/kT})};\ \chi_{\perp} = \frac{Ng_{\perp}^2\mu_B^2\left[1+\frac{3kT}{4D}(1-e^{-2D/kT})\right]}{kT\quad(1+e^{-2D/kT})} \qquad (5)$$

The powder magnetic susceptibility was computed as $\chi = \frac{\chi_{\parallel} + 2\chi_{\perp}}{3}$. With these equations, the temperature dependence of χT was satisfactorily fitted with $g = 2.156(8)$, $D = -3.600(1)$ cm^{-1} for the chloride and $g = 2.171(6)$, $D = -3.392(3)$ cm^{-1} for the iodide derivative. The results of this fit are shown in Figure 3 as a solid line. The temperature dependence of the magnetic susceptibility is independent of the sign of the zfs parameter D. The negative sign was derived by the single-crystal measurements and HF-EPR spectra (vide infra).

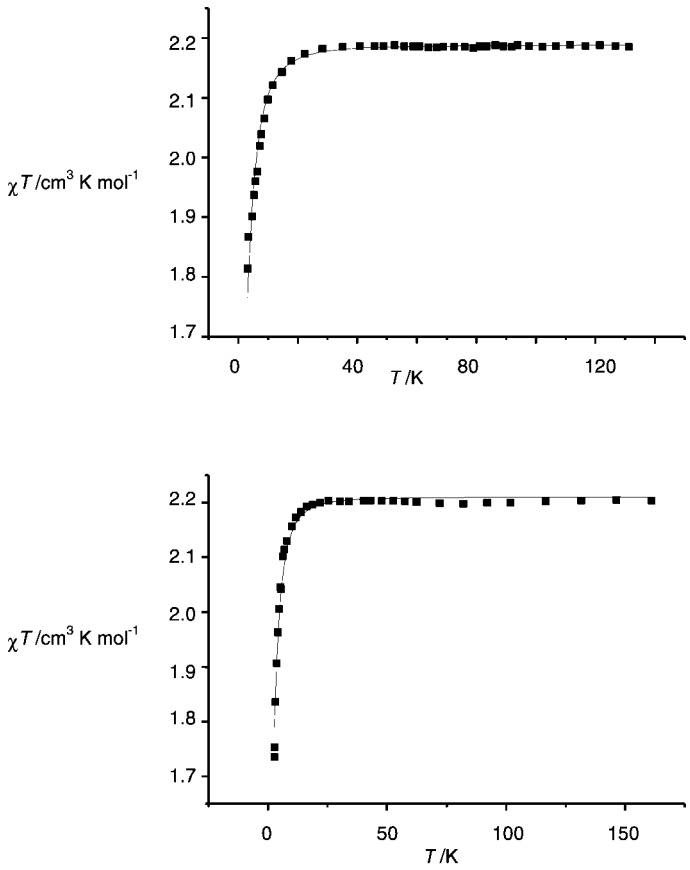

Figure 2. Temperature dependence of the magnetic susceptibility of $[Ni_2(napy)_4Cl_2]^+$ (top) and $[Ni_2(napy)_4I_2]^+$ (bottom) in the form of χT versus T plots. Solid lines are the computed curves with the procedure and parameters described in the text.

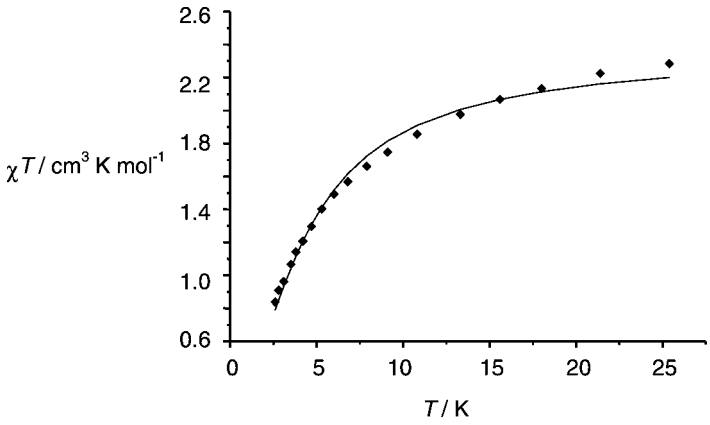

Figure 3. Temperature dependence of the magnetic susceptibility of a single crystal of $[Ni_2(napy)_4Br_2]^+$ in the form of a χT versus T plot. The computed curve is represented as a solid line.

For the bromide derivative it was possible to measure the magnetic susceptibility of a small single crystal. The external magnetic field was close to the perpendicular of the Ni1–Ni2 bond direction. The temperature dependence of χT in the range 2.4–30 K is shown in Figure 3. It gradually decreases from 2.2 emu mol^{-1} K at 30 K to 0.8 emu mol^{-1} K at 2.4 K. The data were fitted using Equation (5) for $\chi_{\perp}$ with $g_{\perp} = 2.26$, $D = -3.3$ cm^{-1}. The results of the fit are shown in Figure 3 as a solid line. The fit is acceptable but not perfect. This can be due to the non-perfect alignment of the crystal along the x-y axis, or to the presence of in-plane anisotropy and/or weak interdimer interactions.

EPR spectra: The X- and Q-band EPR spectra of $[Ni_2(napy)_4Br_2]^+$, recorded at 4.2 K, were previously reported.[9c] They were interpreted with an effective $S=1/2$ spin Hamiltonian with $g_\parallel=2.20-2.22$ and $g_\perp=4.30-4.27$ for the X- and Q-band, respectively. These values originate from the ground $S=3/2$ state with a zero-field splitting larger than the microwave quantum of $\approx 1\ cm^{-1}$ at Q-band. The 4.2 K polycrystalline powder X-band spectra of the chloride and iodide derivatives looks similar with $g_\parallel=2.10$, $g_\perp=4.20$ for the chloride, and $g_\parallel=2.20$ and $g_\perp=4.13$ for the iodide.

The polycrystalline powder spectra of the chloride and of the iodide derivative recorded at 245 GHz are much more informative, in accordance with the fact that at the high frequency, which corresponds to approximately 8.2 cm^{-1}, the transitions between the two split Kramers doublets of the ground $S=3/2$ state are observed. The measured temperature dependence of the HF-EPR spectra of $[Ni_2(napy)_4I_2]^+$ is shown in Figure 4. This dependence is consistent with a negative value of D as shown in Figure 5, where the computed temperature dependence of the spectra is shown for $D=\pm 2.7\ cm^{-1}$. The spectra at 20 K of the chloride and the iodide derivatives were fitted with an $S=3/2$ spin Hamiltonian with $g_\parallel=2.18$, $g_\perp=2.12$, $D=-2.7\ cm^{-1}$, for both compounds, in reasonable agreement with the magnetic data. Using these parameters to simulate the polycrystalline powder spectrum at the X-band (9.3 GHz) we obtained an axial spectrum which could be interpreted with an effective $S'=1/2$ spin Hamiltonian with $g_\parallel=2.18$, $g_\perp=4.18$ in reasonable agreement with the experimental data.

In Figure 6, the measured and computed spectrum of $[Ni_2(napy)_4I_2]^+$ is shown together with the computed dependence of the transition fields and the assignment of the transitions at $\vartheta=0°$. The spectra were simulated by using the computer program developed by Weihe et al.[21] with a Lorentzian line shape with an isotropic line width of 400 Gauss. The angular dependence of the transition fields was computed using the eigenfield formalism.[22]

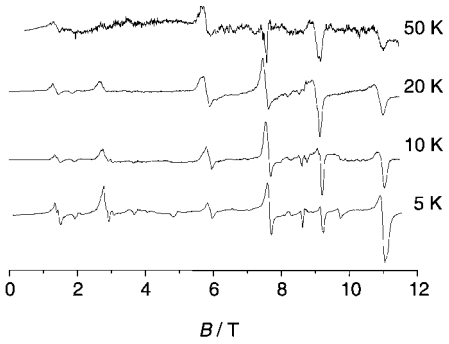

Figure 4. Measured temperature dependence of the polycrystalline powder HF-EPR (245 GHz) spectra of $[Ni_2(napy)_4I_2]^+$.

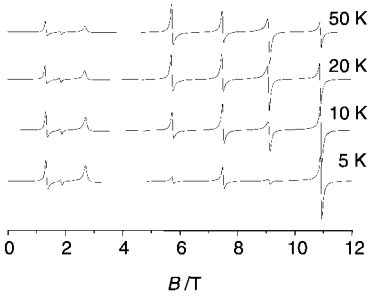

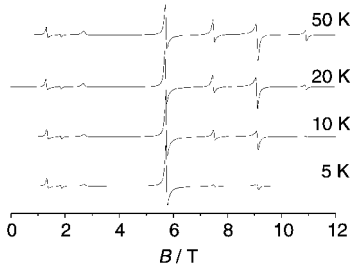

Figure 5. Temperature dependence of polycrystalline powder HF-EPR (245 GHz) spectra of $[Ni_2(napy)_4I_2]^+$ computed by using a $S=3/2$ spin Hamiltonian with $g_\parallel=2.18$, $g_\perp=2.12$, $|D|=2.7\ cm^{-1}$. A Lorentzian lineshape was assumed with a linewidth of 400 Gauss. Top: spectra computed with $D=-2.7 cm^{-1}$. Bottom: spectra computed with $D=2.7 cm^{-1}$.

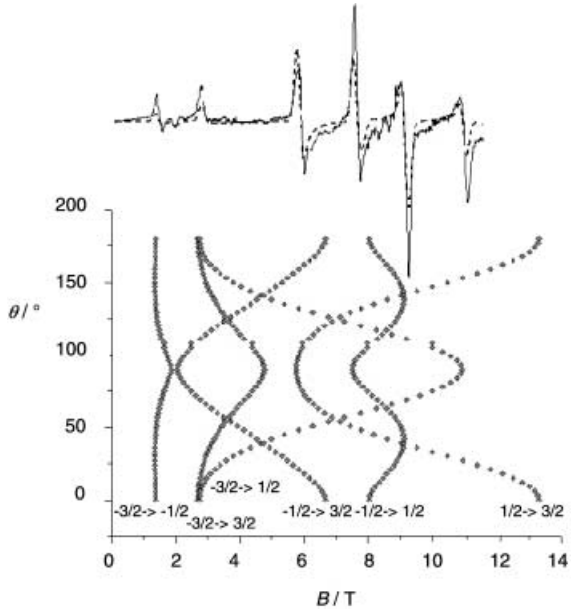

Figure 6. Polycrystalline powder HF-EPR (245 GHz) spectra of $[Ni_2(napy)_4I_2]^+$ recorded at 4.2 K. Top: Experimental spectrum (solid line) and simulated spectrum (dashed line) with a $S=3/2$ spin Hamiltonian with $g_\parallel=2.18$, $g_\perp=2.12$ and $D=-2.7\ cm^{-1}$. Bottom: Computed angular dependence of the transition fields in the xz plane. The assignment of the transitions along z ($\vartheta=0°$) is also shown.

Electronic structure and magnetic properties of $[Ni_2(napy)_4X_2]^+$ (X = Cl,Br,I): The geometry of the $[Ni_2(napy)_4X_2]^+$ (X = Cl, Br, I) complexes was optimized in the idealized D_2 symmetry on the high-spin state ($S=3/2$). The most relevant geometrical parameters are reported in Table 2 where they are also compared to the available experimental data. The agreement with the experimental data is good. The geometry of the iodide derivative was also optimized using the gradient-corrected BLYP functional (Table 2). The computed bond lengths are significantly longer than the experimental ones, and we therefore keep the LDA geometries in the rest of the paper.

0947-6539/02/0816-3664 $ 20.00+.50/0 *Chem. Eur. J.* **2002**, *8*, No. 16

Table 2. Relevant geometrical parameters[a] computed for $[Ni_2(napy)_4X_2]^+$ (X = Cl, Br, I) in D_2 symmetry.

Parameter	X = Cl	X = Br	X = I	X = I[b]
Ni–Ni	2.42	2.41(2.41)	2.41(2.40)	2.49
Ni–X	2.36	2.56(2.64)	2.83(2.92)	3.07
Ni–N	2.06	2.06(2.10)	2.06(2.09)	2.18
$(N\text{-}Ni\text{-}N)_{cis}$	90	90(90)	89(90)	89
$(N\text{-}Ni\text{-}N)_{trans}$	171	171(172)	169(171)	170
N-Ni-X	95	95(94)	95(94)	94
N-Ni-Ni	85	85(86)	84(86)	85
τ[c]	29	28(25)	31(28)	25

[a] Distances in Å, angles in deg (°). Experimental values are shown in parenthesis. The values are averaged over nonequivalent atoms. [b] Geometry optimized using the BLYP functional. [c] Twist angle between the two tetragonal pyramids.

The computed molecular orbitals close to the Fermi level for $[Ni_2(napy)_4I_2]^+$ are shown in Figure 7. In Figure 7 the α and β counterpart of the molecular orbitals are connected with broken lines. The ground configuration is $28b_1^{\downarrow}29b_1^{\downarrow}29a^1$ corresponding to the spin state $S = 3/2$. The computed average

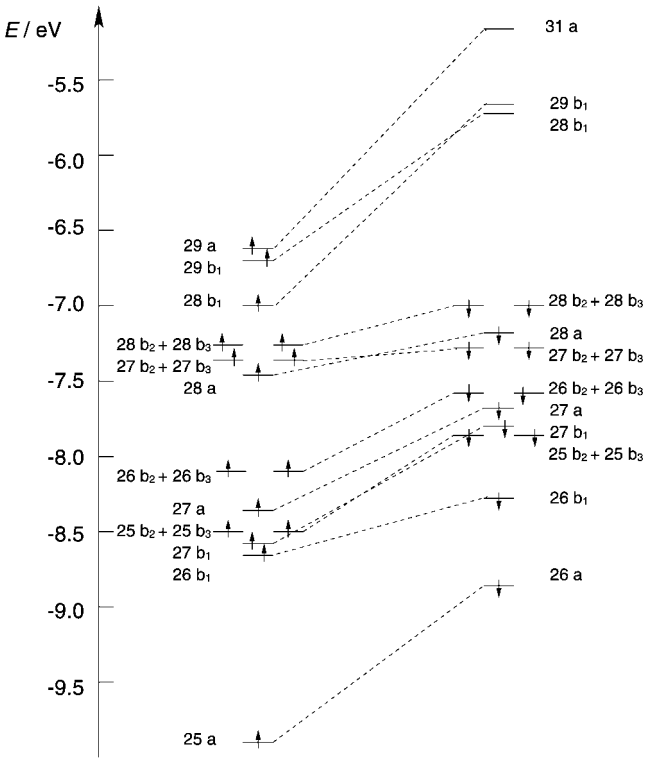

Figure 7. Relative spacing of the molecular orbitals near the Fermi level computed for $[Ni_2(napy)_4I_2]^+$ by using an unrestricted LDA calculation. Spin up (α) orbitals are grouped on the left hand side. Broken lines connect α and β counterparts.

values of $\boldsymbol{S}^2$, $<\boldsymbol{S}^2>$, are 3.78, 3.78, and 3.77 for the Cl^-, Br^-, and I^- derivatives, respectively.[23] These values are very close to $S(S+1)$ indicating a negligible contamination of excited states into the ground state Slater determinant. The composition of the SOMOs, and of the β-LUMOs is shown in Figure 8 as isosurfaces corresponding to a value of the wavefunction ψ of 0.05 a.u. These orbitals correspond to our qualitative picture of Scheme 2 and can be labeled as δ_u

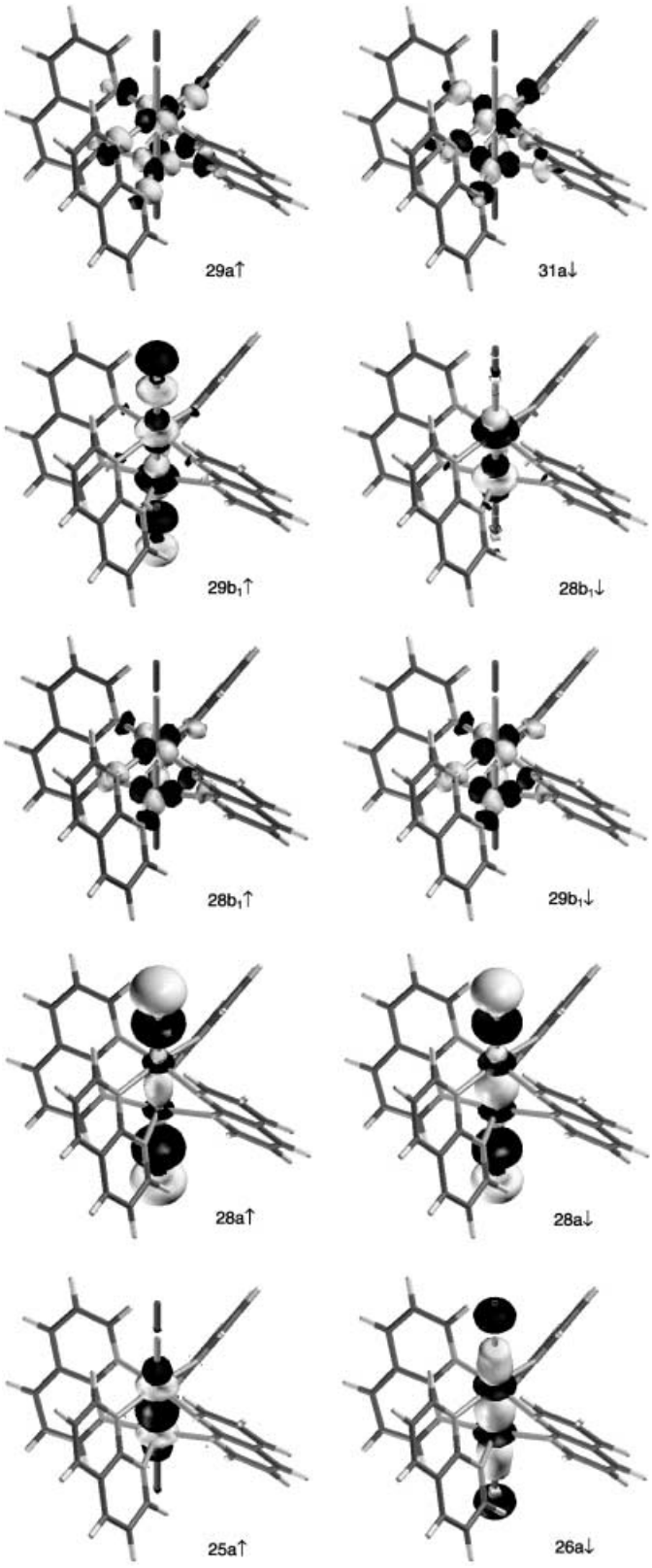

Figure 8. Isosurface representation of the most relevant molecular orbitals discussed in the text. The surfaces correspond to $\psi = \pm 0.05$ a.u.

($28b_1$), σ_u ($29b_1$), and δ_g (29a). The σ_u shows a significant antibonding contribution from the p_z orbitals of the halogen. Two low-lying doubly occupied orbitals (25a and 28a) show significant contribution from the d_{z^2} orbitals of Ni and can be

assigned as the σ_g-type orbital of Scheme 2. Their composition is also shown in Figure 8 and indicates some metal–metal bonding interactions between the nickel atoms. The 28a orbital shows a relevant contribution of the p_z orbitals of the halogen and is closer in composition to the $29b_1$ orbital (σ_u-type orbital). The orbital $26b_1$ is essentially a Ni–I bonding orbital. The orbitals $27b_1$ and the 27a are, respectively, the in-phase and out-of-phase linear combinations of the d_{xy} orbitals of Ni. The degenerate b_2 and b_3 pairs of orbitals are linear combinations of d_{xz} or d_{yz} orbitals of the Ni atoms, with some contributions from the p_x or the p_y orbitals of iodine. A similar energy scheme was computed for the Cl and Br derivatives with the exceptions that the order of the $28b_1$ and $29b_1$ β orbitals was reversed.

The electronic transitions were computed in D_2 symmetry using the Slater's transition state theory performing one-electron excitations from relevant occupied β orbitals to the empty β orbitals $28b_1$ and 31a. Within this formalism it is not possible to compute the oscillator strength of the transitions. The results of the calculations performed on $[Ni_2(napy)_4I_2]^+$ are compared with the experimental spectrum in Table 3. The

Table 3. Computed one-electron transitions (cm^{-1}) for $[Ni_2(napy)_4I_2]^+$.

One-electron excitations	Description[a]	Calcd	Exptl
$28b_2 \rightarrow \sigma_u$	$\lvert d_{xz}-p_x>_+$	10034	9300
$28b_2 \rightarrow \delta_g$	$\lvert d_{xz}-p_x>_+$	12389	
$28a \rightarrow \sigma_u$	$\lvert d_{z^2}-p_z>_+$	13042	15600
$27b_1 \rightarrow \delta_g$	$\lvert d_{xy}>_+$	21398	22200
$25b_2 \rightarrow \delta_g$	$\lvert d_{xz}>_-$	23020	
$26a \rightarrow \sigma_u$ [b]	$\lvert d_{z^2}+p_z>_+$	25680	29000

[a] The principal atomic orbitals forming the starting one-electron molecular orbitals are shown. The notations $\lvert >_+$ and $\lvert >_-$ indicate in-phase and out-of-phase linear combinations of the orbitals centered on the Ni atoms; the signs + and – in the bracket indicate in-phase and out-of-phase combinations of the orbitals of iodine. [b] Short hand notation for $28b_1$ and 31a (see text). Transition $26a \rightarrow 29b_1$ (δ_u) differs by only $\approx 400\ cm^{-1}$ from the $26a \rightarrow 28b_1$. Only the transitions to $28b_1$ have been therefore computed. Also the transitions involving the b_2 and b_3 states are almost degenerate and only one of them is indicated.

$28a \rightarrow \sigma_u$ and $26a \rightarrow \sigma_u$ transitions originate from the bonding combination of the d_{z^2} of Ni that interact with the corresponding linear combination of p_z orbitals of iodine. The Ni–I antibonding interaction shifts the 28a orbital to higher energy. These two transitions were computed also for the Cl and Br derivatives yielding: $26a \rightarrow \sigma_u$ at 33753 and 31053 and $28a \rightarrow \sigma_u$ at 14865 and 14331 for Cl and Br, respectively. The value of the electron transfer parameter B can be computed by using Equation 3 from the $28a \rightarrow \sigma_u$ transition as 3716, 3583, and 3261 cm^{-1} for the Cl, Br, and I derivatives, respectively.

The complete modeling of mixed-valence systems requires the knowledge of the potential energy surface of the system as a function of the position of the atomic nuclei. Only in this way it is possible to estimate the degree of delocalization of the "extra" electron. In the simplest model of the valence trapping, that is, two uncoupled harmonic oscillators centered on the two metal centers, the localization of the "extra" electron is bound to the antisymmetrical breathing vibration, Q, of the whole molecule, which can be viewed as an expansion of one of the two chromophores and a contraction of the other. In previous papers[13, 14] we showed that this Q coordinate could be nicely modeled by following the geometrical rearrangements of the molecules upon displacement of the bridging groups from the equilibrium geometry, the variation of the position of the other ligands being very small. Since in the present complex the bridging ligands are quite rigid we performed a series of geometrical optimizations on $[Ni_2(napy)_4I_2]^+$ by displacing the terminal iodine ligands by their equilibrium positions as shown in Scheme 3, with fixed

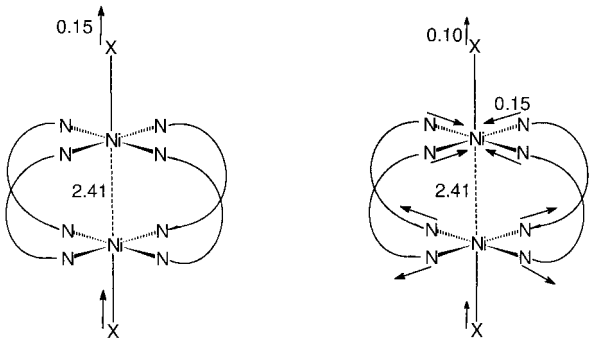

Scheme 3.

Ni–Ni distance at 2.41 Å. All the other geometrical parameters were free of variation. This geometrical variation was represented by the coordinate Q_I, computed as the difference between adjacent geometries in mass-weighted coordinates. In this way we constructed an adiabatic potential energy surface (PES). The computed PES, plotted in Figure 9, is very

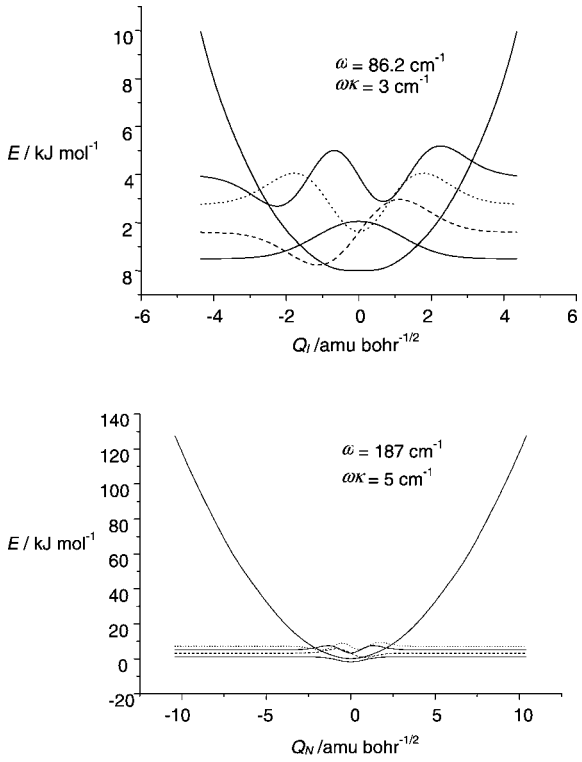

Figure 9. Computed potential energy surfaces (PES) along the Q_I and Q_N nuclear displacements shown in Scheme 3. The harmonic frequencies (ω) and the anharmonic correction ($\omega\kappa$) are indicated together with the spatial extension of the low-lying vibrational levels.

0947-6539/02/0816-3666 $ 20.00+.50/0 *Chem. Eur. J.* **2002**, *8*, No. 16

close to a parabola and the systems can achieve complete delocalization through this motion. The computed overall displacements of the nitrogen atoms of the naphtyridine ligands (see Scheme 3) is only 0.002 Å, showing that Q_I is almost independent of the vibrations of the nitrogen atoms. We have also computed the PES obtained by varying the position of the nitrogen ligands by a fluctuation of the naphtyridine ring around the center of the central C–C bond, with Ni–Ni fixed at 2.41 Å. This movement, also schematically shown in Scheme 3, causes a basal contraction of the four N atoms on one center and the consequent elongation on the other. The computed deviation of the I atoms from their equilibrium position is now relevant, ± 0.1 versus ± 0.15 Å of the N atoms, since from a contraction of the basal atoms an elongation of the axial iodine atoms follows. Also this PES (Figure 8) is very close to a parabola and also this coordinate, Q_N, is active for the determination of the complete delocalization of the "extra" electron. From this PES, effective one-dimensional Schrödinger equations for the motion of a particle with a unitary mass can be computed.[24] This equation can be numerically solved to give anharmonic frequencies associated to this motion. Of course, the structures issuing from electronic calculations must be properly oriented in order to eliminate spurious rotational components.[25] All these steps are fully automated in the program package DiNa.[26] The vibrational frequencies computed by the above approach are also shown in Figure 3. The motion is very close to a harmonic oscillation (the anharmonicity is less than 3.5 %) and the force constants corresponding to the harmonic component are $k_I = 220\ \mathrm{cm^{-1}\,\AA^{-2}}$, and $k_N = 1040\ \mathrm{cm^{-1}\,\AA^{-2}}$ for Q_I and Q_N respectively.

The exchange parameter J can be computed as $J = 2[E(3/2) - E(1/2)]/3$. The energy of the $S = 3/2$ state can be computed using Equation (3) and the calculated B values. The calculation of the doublet state can be performed by using a number of different techniques[13] and a comparison between the various formalisms is in progress. Using the direct calculation of the doublet state through spin unrestricted calculations the following values of J were obtained: 2316, 2116, and 952 $\mathrm{cm^{-1}}$ for the Cl, Br and I derivatives, respectively. From Equation (3), the quartet $E(3/2)$ state is the ground state with the next excited state, $E(1/2)$, at 242, 408, and 1832 $\mathrm{cm^{-1}}$, for Cl, Br, and I, respectively.

In transition metal compounds, the spin-orbit coupling interaction, by admixing states with different spin multiplicity, effectively removes the degeneracy of the spin multiplets in zero field, leading to the zero-field splitting.[27] Although other factors can influence the magnitude of the zfs parameter D, such as spin–spin interactions, they are generally negligible with respect to the spin–orbit coupling contribution. In DFT, spin–orbit coupling can be included by using the relativistic Hamiltonian, which can be approximately solved, for example, with the ZORA method.[28] The resulting one-electron states represent mixed spin states according to the double group symmetry of the molecule. While, in principle, these wavefunctions may be used to solve the multiplet structure of a many electron system, in atomic cases, a precision of 0.2 eV was estimated for these methods, which seems to be far from the accuracy required in our case.[29] A rationalization of the sign and the magnitude of D can be achieved, however, by vector-coupling arguments using simpler ligand field[26] (LF) arguments. In the vector-coupling formalism[12, 13, 30, 31] the spin vectors, $|SM\rangle$, of a mixed valence dimer can be written in a general form as given in Equation (6), where $|S_iS_jSM\rangle_i$ indicates the spin vectors obtained by the coupling of S_i with S_j with the "extra" electron localized on the I center.

$$|SM\rangle = c_A\,|S_AS_BSM\rangle_A + c_B\,|S_AS_BSM\rangle_B \tag{6}$$

In the present case when the "extra" electron is localized on center i we have: $S_i = 1$, $S_j = 1/2$, and $S = 3/2$ for the ground state. Using the formalism already developed one can obtain from Equation (6), Equation (7) in which where $\boldsymbol{D}_S$ is the zfs tensor of the S state and D_s^i is the zfs tensor of the same state when the "extra" electron is localized on i.

$$\boldsymbol{D}_s = c_A^2\boldsymbol{D}_S^A + c_B^2\boldsymbol{D}_S^B \tag{7}$$

For a Class I dimer $C_A = C_b = 1/\sqrt{2}$ and Equation (7) becomes Equation (8).

$$\boldsymbol{D}_S = \frac{1}{2}(\boldsymbol{D}_S^A + \boldsymbol{D}_S^B) \tag{8}$$

In the present case $\boldsymbol{D}_s^i$ can be rewritten as Equation (9), where $\boldsymbol{D}_{s_i}$ is the local zfs of the $S_i = 1$ center and $\boldsymbol{D}_{an}$ is the anisotropic part of the exchange interaction between A and B.

$$\boldsymbol{D}_S^i = \frac{1}{3}(\boldsymbol{D}_{S_i} + \boldsymbol{D}_{an}) \tag{9}$$

Since the two centers are equivalent, $\boldsymbol{D}_{s_A} = \boldsymbol{D}_{s_B}$, Equation (8) takes the simpler form given in Equation (10).

$$\boldsymbol{D}_S = \frac{1}{3}(\boldsymbol{D}_1 + \boldsymbol{D}_{an})$$

The anisotropic contribution to $\boldsymbol{D}_S$ can be conveniently decomposed into exchange, $\boldsymbol{D}_{ex}$, and dipolar, $\boldsymbol{D}_d$, contributions.[13] Due to the r^{-3} dependence of the dipolar term, D_d is expected to be close to zero and, assuming two dipoles with $g = 2$ and 4.1 Å apart, it is computed as 0.04 $\mathrm{cm^{-1}}$. The exchange contribution to the zfs is related to the exchange interaction between the ground state on one ion and the excited states of the other, admixed by spin-orbit coupling.[32] This term can be sizeable and negative since the states involved in the exchange interactions are almost orthogonal. The magnitude of D_1 is surely more difficult to evaluate a priori since it is linked to the geometrical environment of the Ni^{II} center and can vary from 0 $\mathrm{cm^{-1}}$ to a few tens of wavenumbers. To estimate this contributions, we performed LF calculations[33] on a chromophore NiN_4IX (where X is a ligand) that mimics the Ni^I center. Since the largest interaction between the Ni atoms is the σ antibonding interaction between the d_{z^2} orbitals, the X ligand was taken as a σ donor with variable e_σ parameters using the angular overlap model of the ligand field.[34] Calculations were performed[35] using reasonable parameters and values taken from literature data,[36] that is, $e_\sigma^N = -4000\ \mathrm{cm^{-1}}$, $e\pi^N/e_\sigma^N = 0.05$, $e_\sigma^I = -2500\ \mathrm{cm^{-1}}$, and $e_\pi^I/e_\sigma^I = 0.25$. The parameters of the nitrogen ligands are appropriate for pyridine and the π interactions

  0947-6539/02/0816-3667 $ 20.00+.50/0

were assumed to be perpendicular to the aromatic rings, while an isotropic π interaction was assigned to I. The computed values of the zfs parameters D are shown in Figure 10 in the form D versus e_σ^X/e_σ^I. For $e_\sigma^X/e_\sigma^I \geq 2$, D becomes negative and rapidly increases. It can be concluded that the observed D value (-2.7 cm^{-1}) can be attributed to a sizeable contribution of the zfs of the Ni^{II} center. For $e_\sigma^X/e_\sigma^I = 3$ the Ni^{II} ion already contributes 40% of the zfs of the ground $S = 3/2$ spin state. Since the iodide ligand is a weak ligand (at the extreme left of the spectrochemical series) this can be considered a lower limit for the single ion contribution.

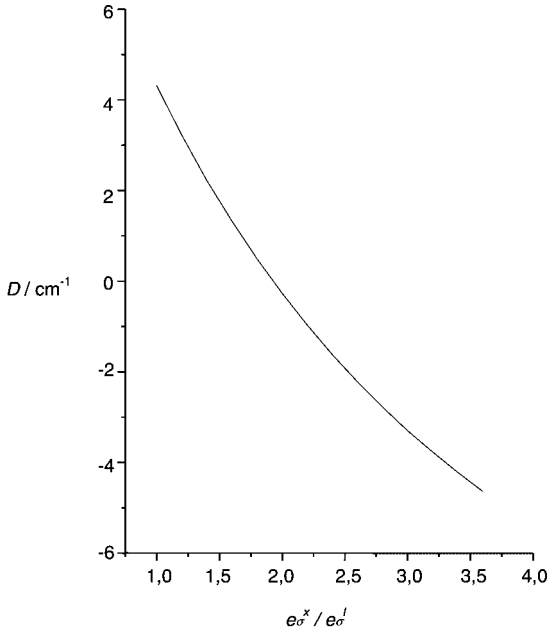

Figure 10. Computed dependence of the single ion zero-field splitting parameter D on e_σ^X/e_σ^I (see text).

Conclusion

DFT has allowed a meaningful comparison of the exchange and double-exchange contributions to the energy separation between the ground $S = 3/2$ and the first excited $S = 1/2$ of the mixed-valence $Ni^{II}-Ni^{I}$ species in $[Ni_2(napy)_4X_2]^+$ (X = Cl, Br, I) cations. The use of high-frequency EPR spectroscopy together with low-temperature magnetic measurements provided an unambiguous description of the zero-field splitting of the ground $S = 3/2$ state, both in terms of the absolute value and sign, which was successfully related to ligand field parameters. The present investigation shows how the combination of DFT calculations and spectroscopic methods may yield important information in mixed-valence compounds. In particular, the characterization of the electron delocalization mechanism can be extracted from the calculation of the adiabatic potential energy surfaces associated to vibrational motions.

Experimental Section

Synthesis of $[Ni(napy)_4X_2]B(C_6H_5)_4$ (X = Cl,Br,I): The complexes were prepared as previously described.[9a, 9b] Single crystals of $[Ni(napy)_4I_2]B(C_6H_5)_4$ suitable for X-ray analysis were obtained by slow diffusion of an acetone solution of the complex with ethanol as precipitating agent.

Elemental analysis calcd (%) for $C_{56}H_{44}N_8BCl_2Ni_2$: C 65.31, H 4.40, N 10.7, Ni 10.9; found: C 65.41, H 4.31, N 10.89, Ni 11.41.

Elemental analysis calcd (%) for $C_{56}H_{44}N_8BBr_2Ni_2$: C 60.13, H 4.28, N 9.56, Ni 9.80; found: C 60.21, H 3.97, N 10.03, Ni 10.50.

Elemental analysis calcd (%) for $C_{56}H_{44}N_8BI_2Ni_2$: C 55.41, H 3.60, N 9.01, Ni 9.60; found: C 55.53, H 3.66, N 9.25, Ni 9.69.

Only crystals of the I^- derivative were found to be of a quality appropriate for X-ray analysis.

XRD data collection and structure determination: Crystals of $[Ni(napy)_4I_2]B(C_6H_5)_4$ were found to be shiny black monoclinic prisms. A crystal of approximate dimensions $0.06 \times 0.4 \times 0.5$ mm was mounted on a glass fiber and transferred to an Enraf–Nonius CAD-4 diffractometer equipped with a graphite-monochromated $Mo_{K\alpha}$ X-ray source ($\lambda = 0.71073$ Å). The unit cell parameters were determined following the method of short vectors followed by least-squares refinement of 25 well-centered reflections. These reflections were also used for monitoring the orientation matrix after every 500 reflections. Data were collected at 293 K using $\omega < 2\Theta$ scan technique. The orientation matrix was recalculated after collecting 500 reflections at a time by centering the same 25 reflections used to start the data collection. Intensities of three standard reflections monitored every 1 h showed no systematic variation. Details concerning crystallographic data collection and structure refinement are summarized in Table 4. Lorentz polarization and empirical (ψ scan) absorption corrections[37] were applied to intensity data. The structure was solved by direct methods and refined by the full-matrix least-squares method on all F^2 data, using the SIR 92[38] and the SHELXL 97[39] programs. All non-hydrogen atoms were refined with anisotropic thermal parameters. Hydrogen atoms were included in calculated positions and refined with isotropic thermal parameters equal to 1.5 those of the parent carbon atoms.

CCDC-175919 contains the supplementary crystallographic data (excluding structure factors) for this paper. These data can be obtained free of charge via www.ccdc.cam.ac.uk/conts/retrieving.html (or from the Cambridge Crystallographic Data Centre, 12 Union Road, Cambridge CB2 1EZ, UK; fax: (+44) 1223-336033; or deposit@ccdc.cam.ac.uk).

Table 4. Crystal data and structure refinement for $[Ni_2(napy)_4I_2]B(C_6H_5)_4$.

empirical formula	$C_{56}\ H_{44}\ B\ I_2\ N_8\ Ni_2$
formula weight	1211.02
temperature [K]	293(2)
wavelength [Å]	0.71069
crystal system, space group	monoclinic, $P2_1/n$
unit cell dimensions	
a [Å]	17.340(5)
b [Å]	26.200(5)
c [Å]	11.340(5)
β [°]	101.320(5)°
volume [Å^3]	5052(3)
Z	4
ρ_{calcd} [mg m^{-3}]	1.592
μ [mm^{-1}]	2.014
$F(000)$	2412
crystal size	$0.06 \times 0.4 \times 0.5$ mm
θ range [°]	2.50–25.49
limiting indices	$0 \leq h \leq 20$, $0 < k \leq 31$, $-13 \leq l \leq 13$
reflections collected/unique	9686/9367 [R(int) = 0.0305]
completeness to theta = 25.49	99.7%
refinement method	full-matrix least-squares on F^2
data/restraints/parameters	9367/0/604
goodness-of-fit on F^2	1.121
final R indices [$I > 2\sigma(I)$]	$R1 = 0.0445$, w$R2 = 0.1308$
R indices (all data)	$R1 = 0.0711$, w$R2 = 0.1731$
largest difference peak and hole [e Å^{-3}]	0.684 and -0.977

0947-6539/02/0816-3668 $ 20.00+.50/0 Chem. Eur. J. 2002, 8, No. 16

Electronic spectra: UV/Vis spectra of $[Ni(napy)_4X_2]B(C_6H_5)_4$ (X = Cl, Br, I) were measured in a dichloromethane solution at room temperature by using a Lambda-9 Perkin–Elmer spectrometer. The molar concentration ($mol\,L^{-1}$) of the solutions was 1.9×10^{-4}, 3.0×10^{-4}, and 3.9×10^{-4} for the Cl, Br, and I derivative, respectively. The absorption maxima (cm^{-1}) with ε ($M^{-1}cm^{-1}$) in parenthesis were: $[Ni(napy)_4Cl_2]B(C_6H_5)_4$: 9.9 (100), 16.6 (2900), 24.1 (3900), 25.3 (3950); $[Ni(napy)_4Br_2]B(C_6H_5)_4$: 9.7 (105), 16.4 (2250), 24.7 (sh), 25.8 (2900); $[Ni(napy)_4I_2]B(C_6H_5)_4$: 9.3 (100), 15.6 (4500), 22.2 (sh), 29.0 (6800).

Magnetic measurements: Temperature dependence of the magnetic susceptibility for $[Ni(napy)_4X_2]B(C_6H_5)_4$ (X = Cl, Br, I) was measured on polycrystalline powders in the temperature range 2.5–150 K with a SQUID magnetometer from Metronique Ingegnerie MS02 with a constant magnetic field of 1 T. Magnetic susceptibilities were corrected for diamagnetism using Pascal's constants.[40] The temperature dependence of $[Ni(napy)_4Br_2]B(C_6H_5)_4$ in the range 2.4–22 K was also measured on a single crystal of 0.85 mg with the static magnetic field of 0.1 T perpendicular to the [0 −1 0] crystallographic face, that is, almost perpendicular to the Ni–Ni direction.

EPR spectra: X-band (9.3 GHz) electron paramagnetic resonance spectra were recorded on polycrystalline powders of $[Ni(napy)_4X_2]B(C_6H_5)_4$ (X = Cl, Br, I) with a Varian E-9 spectrometer equipped with an Oxford Instruments continuous flow cryostat. High-field EPR (HF-EPR) spectra were recorded at 245 GHz on polycrystalline powders of $[Ni(napy)_4X_2]B(C_6H_5)_4$ (X = Cl, I) in the temperature range 4–50 K with an EPR spectrometer built by the Service national des Champs Intenses, CNRS, Grenoble, France.

Computational methods: All the calculations were performed using the Amsterdam Density Fuctional (ADF) program package.[41] Calculations were performed using the local density approximation (LDA) and the generalized gradient approximation (GGA). In the LDA calculations the Xα functional[42] was used for the exchange, the local Vosko, Wilk and Nusair[43] functional was used for the correlation part and the Stoll correlation correction[44] was always applied. GGA calculations were performed by using the nonlocal correction of Becke[45] to the Xα exchange functional and the correlation corrections by Lee, Yang, and Parr[46] (BLYP). The standard basis sets provided within the ADF2000.02 distribution were used throughout. The Frozen Core (FC) approximation for the inner core electrons was adopted. The orbitals up to 1s for carbon and nitrogen, 2p for chlorine, 3p for nickel, 3d for bromine, and 4d for iodine were kept frozen. Hydrogen atoms were treated with a double-ζ basis. Valence electrons on carbon and nitrogen atoms were treated with double-ζ functions. Valence electrons on nickel and halide atoms were treated with triple-ζ functions. The valence shells of carbon, nitrogen, chlorine, and bromine atoms were expanded with single-ζ d polarization functions. Electronic transitions were computed by applying Slater's transition-state theory.[42] The anharmonic frequencies needed for the estimation of vibronic couplings were computed with the DiNa package.[47]

Acknowledgements

We thank Dr. A. L. Barra, CNRS, Grenoble (France), for recording the HF-EPR spectra and Dr. F. Mariotti, University of Fribourg (Switzerland), for his assistance during the calculations. This work was supported by MIUR under the national project "Molecular nanotechnologies for magnetic and non-linear optical materials" 2001, by EC networks: MOLNANOMAG (contract HPRN-CT-1999-00012), 3MD (contract ERBFMRXCT980181), and SENTINEL (contract HPRI-CT-2000-40022), CNR PF MSTA II, Nanotechnologies INFM P.R.A., and COST D9 Action.

[1] J. B. Goodenough, *Progr. Solid State Chem.* **1971**, *5*, 145.
[2] E. Coronado, C. J. Gomez-Garcia, *Comments Inorg. Chem.* **1995**, *17*, 255.
[3] E. L. Bominaar, S. A. Borshch, J.-J. Girerd, *J. Am. Chem. Soc.* **1994**, *116*, 5362.
[4] a) K. D. Jordan, M. N. Paddon-Row, *Chem. Rev.* **1992**, *92*, 395; b) M. D. Newton, *Chem. Rev.* **1991**, *91*, 767; c) K. Prassides, *Mixed Valence Systems: Applications in Chemistry, Physics and Biology*, NATO ASI, Kluwer, Dordrecht, **1991**; d) K. V. Mikkelsen, M. A. Ratner, *Chem. Rev.* **1989**, *87*, 113; e) D. B. Brown, *Mixed Valence Compounds*, NATO ASI, Dordrecht, **1980**.
[5] a) *Electron Transfer in Biology and the Solid State* (Eds.: M. K. Johnson, R. B. King, D. M. Kurtz Jr., C. Kutal, M. L. Norton, R. A. Scott), ACS *226*, Washington DC, **1990**; b) *Electron Transfer in Inorganic, Organic, and Biological Systems* (Eds.: J. R. Bolton, N. Mataga, G. McLendon), ACS *228*, Washington DC, **1991**; c) N. S. Hush, *Progr. Inorg. Chem.* **1967**, *8*, 391; d) S. B. Piepho, E. R. Krausz, P. N. Schatz, *J. Am. Chem. Soc.*, **1978**, *100*, 2996; e) K. Y. Wong, P. N. Schatz, *Progr. Inorg. Chem.*, **1981**, *28*, 369.
[6] a) C. Zener, *Phys. Rev.*, **1951**, *82*, 403; b) P. W. Anderson, H. Hasegawa, *Phys. Rev.*, **1955**, *100*, 675; c) G. Blondin, J.-J. Girerd, *Chem. Rev.*, **1990**, *90*, 1359.
[7] C. N. R. Rao, *J. Phys. Chem.* **2000**, *104*, 5877.
[8] E. L. Bominaar, Z. Hu, E. Münck,; J.-J. Girerd, S. A. Borsch, *J. Am. Chem. Soc.* **1995**, *117*, 6976.
[9] a) D. Gatteschi, C. Mealli, L. Sacconi, *J. Am. Chem. Soc.* **1973**, *95*, 2736; b) L. Sacconi, C. Mealli, D. Gatteschi, *J. Am. Chem. Soc.* **1973**, *95*, 2736; c) A. Bencini, D. Gatteschi, L. Sacconi, *Inorg. Chem.* **1978**, *17*, 2670.
[10] R. L. Martin in *New Pathways in Inorganic Chemistry* (Eds. E. A. V. Ebsworth, A. Maddock, A. G. Sharpe), Cambridge University Press, Cambridge, **1968**.
[11] J.-J. Girerd, *J. Chem. Phys.* **1983**, *79*, 1766.
[12] M. B. Robin, P. Day, *Adv. Inorg. Chem. Radiochem.* **1967**, *10*, 247.
[13] A. Bencini, D. Gatteschi in *Electron Paramagnetic Resonance Spectroscopy* in *Inorganic Electronic Structure and Spectroscopy Vol. I* (Eds.: E. I. Solomon, A. B. P. Lever), Wiley **1999**, 93.
[14] I. Ciofini, C. A. Daul, A. Bencini, in *Recent Andvances in Density Functional Methods, Vol. 1* (Eds.: V. Barone, A. Bencini, P. Fantucci), World Scientific: Singapore, **2001**, Part III, p. 103.
[15] a) A. Bencini, I. Ciofini, C. A. Daul, A. Ferretti, *J. Am. Chem. Soc.* **1999**, *121*, 11418; b) V. Barone, A. Bencini, I. Ciofini, C. A. Daul, F. Totti, *J. Am. Chem. Soc.* **1998**, *120*, 8357; c) V. Barone, A. Bencini, D. Gatteschi, F. Totti, *Chem. Eur. J.* **2002**, *8*, in press.
[16] M. Wolfsberg, L. Helmholtz, *J. Chem. Phys.* **1952**, *20*, 837.
[17] C. J. Calzado, J.-P. Malrieu, J. F. Sanz, *J. Phys. Chem. A* **1998**, *102*, 3659.
[18] The Heisenberg spin Hamiltonian is used in the form $H = J\boldsymbol{S}_1\cdot\boldsymbol{S}_2$. An antiferromagnetic interaction is therefore characterized by a positive value of J.
[19] Equation (4) was derived for a $(n+1)$-particle system, $d^n - d^{n+1}$, where the particles are electrons for $n+1\le5$ and holes for $n+1\ge6$. In the present d^8-d^9 case, therefore, $S_0 = 1/2$ and $B = t_{ab}/2$.
[20] O. Kahn, *Molecular Magnetism*, VCH, New York (USA), **1993**.
[21] a) J. Glerup, H. Weihe, *Acta Chem. Scand.* **1991**, 444. b) C. J. H. Jacobsen, E. Pedersen, J. Villadsen, H. Weihe, *Inorg. Chem.* **1993**, 1216.
[22] G. G. Belford, R. L. Belford, J. F. Burkhalter, *J. Magn. Reson.* **1973**, *11*, 251.
[23] The calculation of $<S^2>$ was performed with the computer program developed by Fabio Mariotti, Université de Fribourg (Switzerland).
[24] V. Barone, C. Minichino, *Theochem* **1995**, *330*, 325.
[25] V. Barone, C. Adamo, *Chem. Phys. Lett.* **1995**, *241*, 1.
[26] DiNa Program, Release 2.1, by V. Barone, University of Naples (Italy).
[27] J. S. Griffith, *The Theory of Transition-Metal Ions*, Cambridge University Press, Cambridge, **1961**.
[28] a) E. van Lenthe, E. J. Baerends, J. G. Snijders, *J. Chem. Phys.* **1993**, *99*, 4597; b) E. van Lenthe, E. J. Baerends, J. G. Snijders, *J. Chem. Phys.*, **1994**, *101*, 9783; c) E. van Lenthe, J. G. Snijders, E. J. Baerends, *J. Chem. Phys.*, **1996**, *105*, 6505.
[29] E. van Lenthe, PhD Thesis, Vrije Universiteit, Amsterdam (Netherlands), **1996**.
[30] I. Belinsky, *Chem. Phys.* **2000**, *255*, 23.
[31] J. J. Borras-Almenar, J. M. Clemente-Juan, E. Coronado, B. S. Tsukerblat, *Inorg. Chem.*, **1999**, *38*, 6081.
[32] J. Kanamori in *Magnetism, Vol. 1* (Eds.: T. G. Rado, H. Suhl), Academic Press, New York, **1963**, p. 161.
[33] A. Bencini, I. Ciofini, M. G. Uytterhoeven, *Inorg. Chim. Acta*, **1998**, *274*, 90.

[34] A. B. P. Lever, E. I. Solomon in *Ligand Field Theory and the Properties of Transition Metal Complexes* in *Inorganic Electronic Structure and Spectroscopy, Vol I* (Eds.: E. I. Solomon, A. B. P. Lever) Wiley **1999**, p. 1.
[35] The other parameters used in the calculations were: $B = 870$, $C = 3350$, $\zeta = -590$ cm^{-1}.
[36] A. Bencini, C. Benelli, D. Gatteschi, *Coord. Chem. Rev.*, **1984**, *60*, 131.
[37] A. C. T. North, D. C. Philips, F. S. Mathews, *Acta Crystallogr. Sect. A* **1968**, *24*, 351.
[38] A. Altomare, M. C. Burla, M. Camaldi, G. Cascarano, C. Giacovazzo, A. Guagliardi, G. Polidori, *J. Appl. Crystallogr.* **1994**, *27*, 435.
[39] G. M. Sheldrick, SHELXL-97, Program for Crystal Structure Refinement, **1997**, University of Göttingen (Germany), Release 97–2.
[40] J. O'Connor, *Prog. Inorg. Chem.* **1982**, *29*, 203.
[41] a) Amsterdam Density Functional (ADF), release 2000.01, Scientific Computing and Modelling, Theoretical Chemistry, Vrije Universiteit, Amsterdam, **2000**; b) E. J. Baerends, D. E. Ellis, P. Ros, *Chem. Phys.* 1973, *2*, 41; b) L. Versluis, T. Ziegler, *J. Chem. Phys.* **1988**, *322*, 88; c) G. te Velde, E. J. Baerends, *J. Comput. Phys.* **1992**, *99(1)*, 84; d) C. Fonseca Guerra, J. G. Snijders, G. te Velde, E. J. Baerends, *Theor. Chem. Acc.* **1998**, *99*, 391.
[42] J. C. Slater in *Quantum Theory of Molecules and Solids, Vol. 4: Self-Consistent Field for Molecules and Solids*, McGraw-Hill, New York, **1974**.
[43] S. H. Vosko, L. Wilk, M. Nusair, *Can. J. Phys.* **1980**, *58*, 1200.
[44] H. Stoll, C. M. Pavilidou, H. Preuss, *Theor. Chim. Acta* **1978**, *49*, 143.
[45] A. D. Becke, *Phys. Rev. A* **1988**, *38*, 3098.
[46] C. Lee, W. Yang, R. G. Parr, *Phys. Rev. B* **1988**, *37*, 785.
[47] V. Barone in *Recent Andvances in Density Functional Methods, Vol. 1*, (Ed. D. P. Chang), World Scientific, Singapore, **1996**, p. 287.

Received: December 13, 2001
Revised: March 31, 2002 [F3735]

  0947-6539/02/0816-3670 $ 20.00+.50/0